Synthesis, characterization and up-conversion luminescence properties of α-$NaYF_4$:Yb^{3+}/Er^{3+}/PVP/MOFs multilayer nanocrystals

Thi Kieu Giang Lam[1,2*], Lukasz Marciniak[3], Quang Huy Tran[4], Manh Tien Dinh[1], Duc Chinh Vu[1], Vu Nguyen[1], Thu Huong Tran[1], Thi Khuyen Hoang[1], Thanh Huong Nguyen[1], Duc Roan Pham[5], Thanh Binh Nguyen[6], Quoc Minh Le[1,2]

[1]*Institute of Materials Science, Vietnam Academy of Science and Technology*
[2]*Graduate University of Science and Technology, Vietnam Academy of Science and Technology*
[3]*Institute of Low Temperature and Structural Research, Polish Academy of Sciences, Poland*
[4]*National Institute of Hygiene and Epidemiology (NIHE)*
[5]*Faculty of Chemistry, Hanoi National University of Education*
[6]*Laboratory of Photochemistry Imaging and Photonics, Institute of Applied Physics and Scientific Instrument, Vietnam Academy of Science and Technology*

Received 1 June 2017; accepted 5 September 2017

Abstract:

The precursor PVP-capped α-$NaYF_4$:Yb^{3+}/Er^{3+} nanospheres were used as the templates for preparing the α-$NaYF_4$:Yb^{3+}/Er^{3+}/PVP/MOFs multilayer nanocrystals with a self-template method. By using iron (III) carboxylate and zeolitic imidazolate frameworks dissolved in dimethylformamide (DMF) solution containing 25% of diethylene glycol (DEG), the spherical-shaped α-$NaYF_4$:Yb^{3+}/Er^{3+}/PVP/MIL-100 and α-NaYF4:Yb^{3+}/Er^{3+}/PVP/ZIF-8 multilayer nanocrystals were successfully prepared with the sizes of 300-500 nm at 100°C for one hour. Under a 976 nm laser excitation at room temperature, the α-$NaYF_4$:Yb^{3+}/Er^{3+}/PVP/MIL-100 and α-$NaYF_4$:Yb^{3+}/Er^{3+}/PVP/ZIF-8 multilayer nanocrystals exhibited strong up-conversion luminescence with three emission bands centered at around 520 nm, 540 nm, and 655 nm corresponding to $^2H_{11/2} \rightarrow {}^4I_{15/2}$, $^4S_{3/2} \rightarrow {}^4I_{15/2}$, and $^4F_{9/2} \rightarrow {}^4I_{15/2}$ transitions of Er^{3+} ions, respectively.

Keywords: ***metal-organic frameworks, multilayer nanocrystals, self-template method, up-conversion, α-$NaYF_4$:Yb^{3+}/Er^{3+}/PVP/MIL-100, α-$NaYF_4$:Yb^{3+}/Er^{3+}/PVP/ZIF-8.***

Classification numbers: ***5.2, 5.5***

Introduction

Metal-organic frameworks (MOFs) are considered as the new classes of hybrid porous materials assembled with metal cations and organic ligands. Due to their unique physical and chemical characteristics, they have been widely investigated for various applications such as biosensors, gas storage, catalysis, and separation, etc. [1-5]. Particularly, MOFs based on iron (III) carboxylate materials (MIL-100) and/or zeolitic imidazolate framework (ZIF-8) have recently attracted a great deal of attention owing to their prospective applications in drug delivery, diagnostics, and therapy of cancer [6-8].

Recently, rare earth doped $NaYF_4$ nanoparticles (NPs) have been proven to have excellent near-infrared (NIR) excited up-conversion luminescence (UCL) properties, making the new generation of bio-probes in diagnostics and therapy of cancer [9-12]. Stimulated by this discovery, many research groups have been paying their attention to fabricate and study UCL@MOFs nanocrystals for applications in bioimaging, diagnosis, and targeted drug delivery [13, 14].

In this work, a self-template method was used to prepare high-quality

*Corresponding author: Email: giangltk@ims.vast.ac.vn

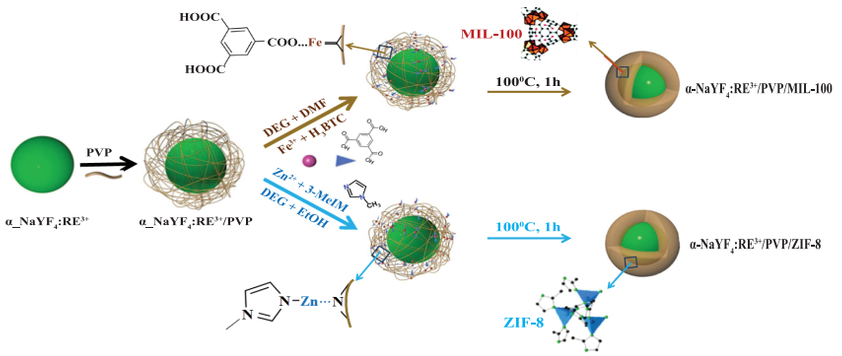

Scheme 1. Schematic illustration of the synthesis of α-$NaYF_4$:Yb^{3+}/Er^{3+}/PVP/MOF multilayer nanocrystals.

multilayer nanocrystals, in which PVP-capped α-$NaYF_4$:Yb^{3+}/Er^{3+} nanospheres were used as the core, and MIL-100 (or ZIF-8) served as shell layers. It hypothesized that the spherical shape of α-$NaYF_4$:Yb^{3+}/Er^{3+}/PVP/MIL-100 and α-$NaYF_4$:Yb^{3+}/Er^{3+}/PVP/ZIF-8 multilayer nanocrystals would exhibit simultaneously both NIR optical property of UCL cores and the unique property of metal-organic frameworks (Scheme 1).

Experimental

Materials

Iron (III) chloride hexahydrate ($FeCl_3 \cdot 6H_2O$, 99.0%), Zinc nitrate tetrahydrate ($Zn(NO_3)_2.4H_2O$, 98.5%), Trimesic acid (H_3BTC), Dimethylformamide (DMF, 99.5%), 3-Methylimidazole (3-MeIM, $C_4H_6N_2$), Diethylene glycol (DEG), Sodium acetate (CH_3COONa), Ammonium fluoride (NH_4F), Rare-earth chlorides ($RECl_3.6H_2O$, RE^{3+}:Y^{3+}, Yb^{3+}, Er^{3+}), polyvinylpyrrolidone (PVP, Mw ~20,000), and hydrogen chloride solution were purchased from Merck and Sigma-Aldrich. All the chemicals were of analytical grade.

Synthesis of PVP-capped α-$NaYF_4$:Yb^{3+}/Er^{3+} nanospheres

The PVP-capped α-$NaYF_4$:Yb^{3+}/Er^{3+} nanospheres were synthesized according to our previous report [15] as follows:

Firstly, three solutions of $YCl_3.6H_2O$, $YbCl_3.6H_2O$, and $ErCl_3.6H_2O$ were mixed by magnetic stirring for one hour (Y^{3+}/Yb^{3+}/Er^{3+} molar ratio of 79/19/2). Then, the solution of CH_3COONa dissolved in DEG was slowly added while being stirred for 30 minutes to obtain solution A. Simultaneously, a solution containing NH_4F was dissolved in DEG and slowly added to the solution A, then stirred until a homogeneous mixture was obtained. The resulting homogeneous mixture was poured into a 100 ml Teflon vessel and heated up at a temperature of 120°C for two hours in the argon atmosphere under vigorous magnetic stirring, and then cooled down to room temperature by ice water. The samples of α-$NaYF_4$:Yb^{3+}/Er^{3+} nanopowders were cleaned by centrifugation with deionized water and isopropanol and dried at 70°C in air.

After that, the α-$NaYF_4$:Yb^{3+}/Er^{3+} nanopowders were re-dissolved into 10 ml HCl (0.1 M) solution, washed three times by ultrasonic treatment and centrifugation. The products of 0.1 g α-$NaYF_4$:Yb^{3+}/Er^{3+} nanoparticles were dissolved in 10 ml ethanol solution containing 0.5 g of PVP (M_w=20000) and vigorously stirred to obtain the homogeneous solution of PVP-capped α-$NaYF_4$:Yb^{3+}/Er^{3+} nanospheres.

Synthesis of α-$NaYF_4$:Yb^{3+}/Er^{3+}/PVP/MOF multilayer nanocrystals

Firstly, the mother solution B was prepared for the secondary growth to form a thick MIL-100 and ZIF-8 layers as follows:

- Mix the solution of 0.05 g of $FeCl_3 \cdot 6H_2O$ and 0.04 g of H_3BTC into 20 ml solution containing 75% of DMF and 25% of DEG under stirring at 25°C for one hour (with MIL-100 layer).

- Mix the solution of 0.2 g of $Zn(NO_3)_2.4H_2O$ and 0.3 g 3-Methylimidazole (3-MeIM) into 20 ml solution containing 75% of ethanol (EtOH) and 25% of DEG under stirring at 25°C for one hour (with ZIF-8 layer).

After that, 10 ml of the prepared solution of PVP-capped α-$NaYF_4$:Yb^{3+}/Er^{3+} nanospheres was dropped into the mother solution B and gently stirred at room temperature for one hour to obtain the homogeneous solution C. The homogeneous solution C was heated up at 100°C for one hour in the argon atmosphere under vigorous magnetic stirring and cooled down to room temperature by ice water.

Finally, the obtained products of α-$NaYF_4$:Yb^{3+}/Er^{3+}/PVP/MOF multilayer nanocrystals were cleaned three times with ethanol by centrifugation to remove redundant iron ions and acid, and then dried at 70°C for 24 hours.

Instrumentation

The crystalline phase structure was determined by using a PANalytical X'Pert Pro diffractometer with Cu K_α radiation (λ = 1.54060 Å) in the 2θ range of from 5° to 70°. The average grain size was calculated by using Scherrer's formula [16]:

$$D = k\lambda/(\beta \cos\theta) \quad (1)$$

where λ is the wave length of the X-ray diffraction, θ is the diffraction angle and β is full width at half maximum (FWHM).

The morphology of the nanocrystals was investigated by FE-SEM (S-4800, Hitachi). Fourier transform infrared spectroscopy (FTIR) analysis was carried out on the Thermo Nicolet NEXUS 670 FTIR (USA). Up-conversion luminescence measurements were performed at room temperature with a Jobin-Yvon HR1000 monochromator,

equipped with a charge-coupled device (CCD) camera using a 976 nm laser diode.

Results and discussions

The α-$NaYF_4$:Yb^{3+}/Er^{3+}/PVP/MOF multilayer nanocrystals were successfully synthesized by using the self-template method at the temperature of 100°C for one hour. The evolution of the crystalline phase of α-$NaYF_4$:Yb^{3+}/Er^{3+}/PVP/MOF multilayer nanocrystals compared with the single crystalline of PVP-capped α-$NaYF_4$:Yb^{3+}/Er^{3+} nanospheres, MOF, and reference crystallographic data of α-$NaYF_4$ (JCPS No. 77-2042) was confirmed by XRD measurements (Fig. 1).

With the samples of PVP-capped α-$NaYF_4$:Yb^{3+}/Er^{3+} nanospheres (patterns $\mathbf{P_1}$ and $\mathbf{P_4}$), all diffraction peaks corresponding to pure cubic α phase of $NaYF_4$ (JCPS No. 77-2042) with a calculated lattice constant are 5.447 Å, space group Fm-3m, and Z=4. Meanwhile, after being mixed with the mother solution for the secondary growth to form a thick MOF layer, the as-synthesized α-$NaYF_4$:Yb^{3+}/Er^{3+}/PVP/MOF multilayer nanocrystals (pattern $\mathbf{P_3}$) have two group peaks which match the standard cubic $NaYF_4$ XRD pattern (JCPS No. 77-2042) and MIL-100 crystalline phase (marked with "*", pattern $\mathbf{P_2}$) [17] or amorphous ZIF-8 (pattern $\mathbf{P_5}$) [18]. In addition, the average grain size calculated by using Scherrer's formula with all samples is around 45 ± 5 nm, suggesting the formation of MOF layer onto the surface of the core α-$NaYF_4$:Yb^{3+}/Er^{3+} nanospheres while maintaining the crystallographic phase of α-$NaYF_4$:Yb^{3+}/Er^{3+} nanospheres.

Figure 2 shows the morphology of α-$NaYF_4$:Yb^{3+}/Er^{3+}/MIL-100 and α-$NaYF_4$:Yb^{3+}/Er^{3+}/PVP/ZIF-8 multilayer nanocrystals obtained at the temperature of 100°C for one hour. As it is shown in the inset of Fig. 2A (S_1), the core of PVP-capped α-$NaYF_4$:Yb^{3+}/Er^{3+} nanospheres has the size of around 40 nm. After being mixed with the mother solutions for the secondary growth to form a thick MOF layer, the α-$NaYF_4$:Yb^{3+}/Er^{3+}/PVP/MIL-100 and α-$NaYF_4$:Yb^{3+}/Er^{3+}/PVP/ZIF-8 multilayer nanocrystals obtained have the sizes of 300-400 nm (Fig. 2A, S_2) and 300-500 nm (Fig. 2B, S_3), respectively. The insets of Fig. 2A (S_2) and Fig. 2B (S_3) confirm the core/shell structures of α-$NaYF_4$:Yb^{3+}/Er^{3+}/MIL-100 and α-$NaYF_4$:Yb^{3+}/Er^{3+}/ZIF-8 multilayer nanocrystals.

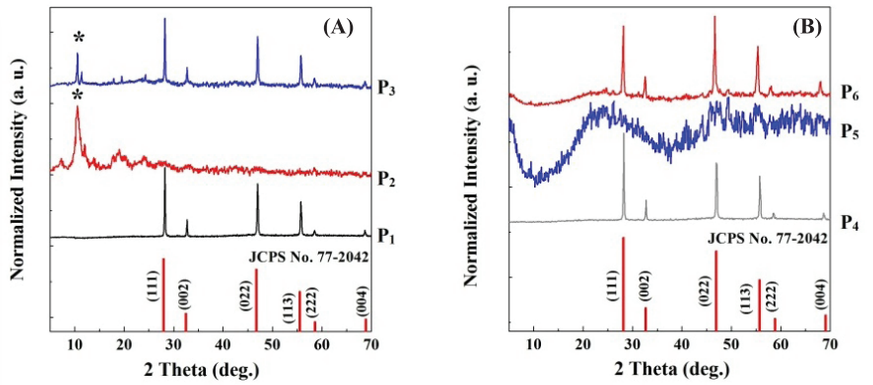

Fig. 1. The normalized XRD patterns of samples: (A) α-$NaYF_4$:Yb^{3+}/Er^{3+}/PVP/MIL-100 multilayer nanocrystals (pattern P_3) compared with PVP-capped α-$NaYF_4$:Yb^{3+}/Er^{3+} nanospheres (pattern P_1) and MIL-100 (pattern P_2) and **(B)** α-$NaYF_4$:Yb^{3+}/Er^{3+}/PVP/ZIF-8 multilayer nanocrystals (pattern P_6) compared with PVP-capped α-$NaYF_4$:Yb^{3+}/Er^{3+} nanospheres (pattern P_4) and amorphous ZIF-8 (pattern P_5). The JCPS No. 77-2042 is the reference crystallographic data of α-$NaYF_4$ (JCPS No. 77-2042) and the peaks of MIL-100 are marked with "*".

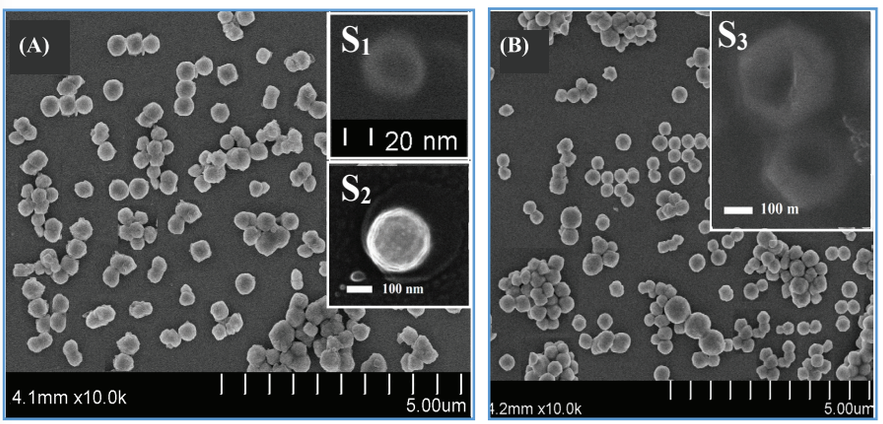

Fig. 2. The FE-SEM images of (A) α-$NaYF_4$:Yb^{3+}/Er^{3+}/MIL-100 and **(B)** α-$NaYF_4$:Yb^{3+}/Er^{3+}/ZIF-8 multilayer nanocrystals prepared by self-template method at the temperature of 100°C for one hour. The inset S_1 shows the core of PVP-capped α-$NaYF_4$:Yb^{3+}/Er^{3+} nanospheres. The insets S_2 and S_3 give the high-magnification SEM image of the samples α-$NaYF_4$:Yb^{3+}/Er^{3+}/MIL-100 and α-$NaYF_4$:Yb^{3+}/Er^{3+}/ZIF-8 multilayer nanocrystals (scale bar: 100 nm).

Figure 3 presents the FTIR spectra of α-$NaYF_4$:Yb^{3+}/Er^{3+}/PVP/MIL-100 (curve a_2) and $NaYF_4$:Yb^{3+}/Er^{3+}/PVP/ZIF-8 (curve b_2) multilayer nanocrystals compared with PVP-capped α-$NaYF_4$:Yb^{3+}/Er^{3+} nanospheres (curves a_1 and b_1), MIL-100 (curve a_3) and ZIF-8 (curve b_3). The characteristic infrared (IR) absorption bands and the corresponding organic functional groups of samples α-$NaYF_4$:Yb^{3+}/Er^{3+}/PVP/MIL-100 *(NP/MIL100)*, MIL-100,

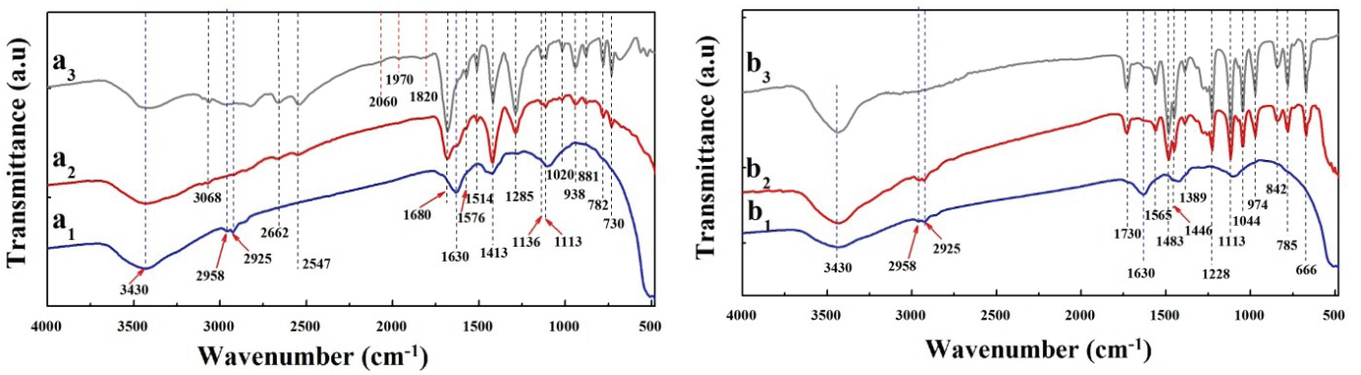

Fig. 3. FTIR spectra of α-$NaYF_4$:Yb^{3+}/Er^{3+}/PVP/MIL-100 (curve a_2) and $NaYF_4$:Yb^{3+}/Er^{3+}/PVP/ZIF-8 (curve b_2) multilayer nanocrystals compared with PVP-capped α-$NaYF_4$:Yb^{3+}/Er^{3+} nanospheres (curves a_1 and b_1), MIL-100 (curve a_3), and ZIF-8 (curve b_3).

and α-$NaYF_4$:Yb^{3+}/Er^{3+} nanospheres *(NP)*, $NaYF_4$:Yb^{3+}/Er^{3+}/PVP/ZIF-8 *(NP@ZIF8)*, and ZIF-8 are illustrated in Table 1.

It can be seen in Fig. 3 and Table 1 that the broad absorption peak at around 3430 cm^{-1} corresponding to hydroxyl groups (-OH) was observed in all samples (curves a_1-a_3 and b_1-b_3). In addition, compared to the spectra of α-$NaYF_4$:Yb^{3+}/Er^{3+} (curve a_1), the spectrum of MIL-100 and α-$NaYF_4$:Yb^{3+}/Er^{3+}/PVP/MIL-100 multilayer nanocrystals has adsorption bands which represent for MIL-100 structure. For example, the strong vibrational bands at around 1285, 1413, and 1680 cm^{-1} corresponding to the symmetric -COOH stretching and interaction between the deprotonated -COOH and the Fe ion indicate the growth of MIL-100 crystals on the surface of the PVP-caped α-$NaYF_4$:Yb^{3+}/Er^{3+} nanospheres [17]. Especially, in the MIL-100 and α-$NaYF_4$:Yb^{3+}/Er^{3+}/PVP/MIL-100 multilayer nanocrystals, we can observe the weak signal in the range of 1820-2060 cm^{-1} bands corresponding to the traces of residual trimesic acid, which proves that the cleaning process by using centrifugation with ethanol is very effective in removing the residual trimesic acid. Furthermore, the characteristic peaks of ZIF-8 observed in both of ZIF-8 (curve b_3) and $NaYF_4$:Yb^{3+}/Er^{3+}/PVP/ZIF-8 (curve b_2) samples suggest the existence of ZIF-8 layer on the surface of the PVP-caped α-$NaYF_4$:Yb^{3+}/Er^{3+} nanospheres [19].

Table 1. The characteristic IR absorption bands of samples α-$NaYF_4$:Yb^{3+}/Er^{3+}/PVP/MIL-100 (*NP/MIL100*), MIL-100, and α-$NaYF_4$:Yb^{3+}/Er^{3+} nanospheres (*NP*), $NaYF_4$:Yb^{3+}/Er^{3+}/PVP/ZIF-8 (*NP@ZIF8*), and ZIF-8 [20].

Characteristic absorptions (cm^{-1})	Functional groups [21]	Intensities: vs-very strong; s-strong; m-medium; w-weak; vw-very weak				
		NP@MIL-100	*MIL-100*	*NP*	*NP@ZIF8*	*ZIF-8*
3430	–OH groups	vs	vs	vs	vs	vs
3068	C–H stretching	vw	vw	-	-	-
2958, 2925	C–H stretching	-	-	w	w	-
2662, 2547	–OH (of DMF)	w	w	-	-	-
2060,1970, 1820	Residual H_3BTC	vw	vw	-	-	-
1730	–C=O stretching	-	-	-	m	m
1680	–COOH stretching	vs	vs	-	-	-
1630	–C=O stretching	w	-	s	w	w
1565	C=C stretching	-	-	-	m	m
1483	Aromatic stretching	-	-	-	vs	vs
1446	C–H stretching	-	-	-	m	m
1413	–COOH stretching	vs	vs	-	-	-
1285	–C=O stretching	s	vs	-	-	-
1228	C–N stretching	-	-	-	vs	vs
1113	C–N stretching	-	-	-	vs	vs
1044	C–N–C stretching	-	-	-	vs	vs
974	C–N stretching	-	-	-	s	s
938	δ(O−H)	m	m	-	-	-
842	C–N stretching	-	-	-	s	s
782	–CH	m	m	-	-	-
730	C–H stretching	m	m	-	-	-
666	C–N stretching	-	-	-	s	s

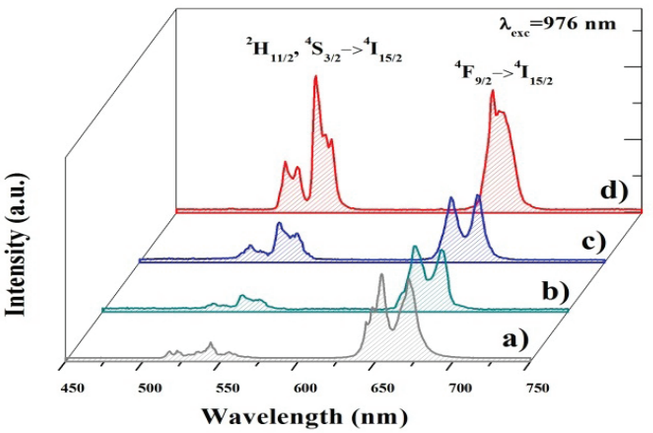

Fig. 4. The comparison of up-conversion luminescence spectra of the α−$NaYF_4$:19%Yb^{3+}/2%Er^{3+}/PVP/MIL-100 and α-$NaYF_4$:19%Yb^{3+}/2%Er^{3+}/PVP/ZIF-8 multilayer nanocrystals compared with the bare core α-$NaYF_4$:19%Yb^{3+}/2%Er^{3+} nanoparticles and PVP-caped α−$NaYF_4$:19%Yb^{3+}/2%Er^{3+} nanospheres upon 976 nm excitation at 800 mW.

Table 2. Integrated emission intensity ratio of the red to green regions of the as-synthesized samples

Sample	I_{Green}	I_{Red}	I_{Green}/I_{Red}
Bare core α-$NaYF_4$:Yb^{3+}/Er^{3+} nanoparticles	0.38	2.82	~ 0.13
PVP-capped α-$NaYF_4$:Yb^{3+}/Er^{3+} nanospheres	0.38	1.90	~ 0.20
α-$NaYF_4$:Yb^{3+}/Er^{3+}/PVP/ZIF-8 multilayer nanocrystals	1.00	1.82	~ 0.55
α-$NaYF_4$:Yb^{3+}/Er^{3+}/PVP/MIL-100 multilayer nanocrystals	2.75	2.73	~ 1.01

The up-conversion luminescence spectra of the α-$NaYF_4$:19%Yb^{3+}/2%Er^{3+}/PVP/MIL-100 and α-$NaYF_4$:19%Yb^{3+}/2%Er^{3+}/PVP/ZIF-8 multilayer nanocrystals compare with the bare core α-$NaYF_4$:19%Yb^{3+}/2%Er^{3+} nanoparticles and PVP-caped α-$NaYF_4$:19%Yb^{3+}/2%Er^{3+} nanospheres upon 976 nm excitation at 800 mW are showed in Fig. 4.

The results revealed that the α-$NaYF_4$:19%Yb^{3+}/2%Er^{3+}/PVP/MIL-100 and α-$NaYF_4$:19%Yb^{3+}/2%Er^{3+}/PVP/ZIF-8 multilayer nanocrystals had three emission bands at around 520 nm, 540 nm, and 655 nm corresponding to $^2H_{11/2} \rightarrow {}^4I_{15/2}$, $^4S_{3/2} \rightarrow {}^4I_{15/2}$, and $^4F_{9/2} \rightarrow {}^4I_{15/2}$ transitions of Er^{3+} ions, respectively. The integrated intensity of UCL emission in green and red spectral regions of as-synthesized samples was shown in Table 2 with the note that all of the data shown in Table 2 were obtained for the same experimental conditions.

The obtained data show that the total integrated emission intensity of the $NaYF_4$:19%Yb^{3+}/2%Er^{3+}/PVP/MIL-100 multilayer nanocrystals is about 1.94 times higher than that of the $NaYF_4$:19%Yb^{3+}/2%Er^{3+}/PVP/ZIF-8 multilayer nanocrystals, and about 1.71 and 2.41 times higher than that of the PVP-caped α-$NaYF_4$:Yb^{3+}/Er^{3+} nanospheres and bare core α-$NaYF_4$:2%Er^{3+},19%Yb^{3+} nanoparticles, respectively. Moreover, when adding the layers of PVP, PVP/ZIF-8 or PVP/MIL-100, the integrated intensity ratio of green to red emissions increased from 0.13 to 1.01. This suggests that the efficiency of the up-conversion increases when increasing the particle size of bare core α-$NaYF_4$:19%Yb^{3+}/2%Er^{3+} nanoparticles, PVP-caped α-$NaYF_4$:19%Yb^{3+}/2%Er^{3+} nanospheres, α-$NaYF_4$:19%Yb^{3+}/2%Er^{3+}/PVP/MIL-100, and α-$NaYF_4$:19%Yb^{3+}/2%Er^{3+}/PVP/ZIF-8 multilayer nanocrystals [21]. The increase in the efficiency of the up-conversion could be speculated due to the porous structure of MIL-100 shells. This leads to the limitation of transferring photo-generated electron–hole pairs in the α- $NaYF_4$:19%Yb^{3+}/2%Er^{3+}/PVP/MIL-100 multilayer nanocrystals.

Conclusions

In summary, a self-template method was utilized to prepare high-quality $NaYF_4$:19%Yb^{3+}/2%Er^{3+}/PVP/MIL-100 and α-$NaYF_4$:19%Yb^{3+}/2%Er^{3+}/PVP/ZIF-8 multilayer nanocrystals. The UCL spectra studies demonstrated that the integrated intensity ratio of green to red emissions increased from 0.13 to 1.01 when adding the layers of PVP, PVP/ZIF-8 or PVP/MIL-100 on the surface of the α-$NaYF_4$:Yb^{3+}/Er^{3+} nanoparticles. This suggests that the efficiency of the up-conversion increases due to the decrease in contribution of the non-radiative processes when an increase in particle size affects the bare core α-$NaYF_4$:19%Yb^{3+}/2%Er^{3+} nanoparticles, PVP-caped α-$NaYF_4$:19%Yb^{3+}/2%Er^{3+} nanospheres, α-$NaYF_4$:19%Yb^{3+}/2%Er^{3+}/PVP/MIL-100, and α-$NaYF_4$:19%Yb^{3+}/2%Er^{3+}/PVP/ZIF-8 multilayer nanocrystals.

ACKNOWLEDGEMENTS

We would like to express our sincere gratitude to Professor Acad. Nguyen Van Hieu (VAST), Prof. Nguyen Quang Liem (VAST), and Prof. Vu Dinh Lam (VAST) for their great support and encouragement to promote the application research of new research directions for metal-organic frameworks

in Institute of Materials Science. This research is funded by Vietnam National Foundation for Science and Technology Development (NAFOSTED) under grant number 103.03-2016.60.

REFERENCES

[1] R.J. Kuppler, D. J. Timmons, Q.R. Fang, J.R. Li, T.A. Makal, M.D. Young, D. Yuan, D. Zhao, W. Zhuang, H.C. Zhou (2009), "Potential applications of metal-organic frameworks", *Coordination Chemistry Reviews*, **253**, pp.3042-3066.

[2] H. Furukawa, K.E. Cordova, M. O'Keeffe, O.M. Yaghi (2013), "The chemistry and applications of metal-organic frameworks", *Science*, **341**, doi:10.1126/science.1230444.

[3] A.C.M. Kinlay, R.E. Morris, P. Horcajada, G. Férey, R. Gref, P. Couvreur, C. Serre (2010), "BioMOFs: Metal-Organic Frameworks for Biological and Medical Applications", *Angew. Chem. Int. Ed.*, **49**, pp.6260-6266.

[4] T.B. Nguyen, M.T. Dinh, T.K.G. Lam, T.K. Hoang, T.H. Nguyen, T.H. Tran, D.L. Tran (2014), "Study on preparation and characterization of MOF based lanthanide doped luminescent coordination polymers", *Materials Chemistry and Physics*, **143**, pp.946-951.

[5] T.B. Nguyen, T.T. Phung, T.H.L. Ngo, M.T. Dinh, T.K. Hoang, T.K.G. Lam, T.H. Nguyen, T.H. Tran, D.L. Tran (2015), "Study on preparation and properties of a novel photo-catalytic material based on copper-centred metal-organic frameworks (Cu-MOF) and titanium dioxide", *Int. J. Nanotechnol.*, **12**, pp.447-455.

[6] S. Keskin and S. Kızılel (2011), "Biomedical Applications of Metal Organic Frameworks", *Industrial & Engineering Chemistry Research*, **50**, pp.1799-1812.

[7] W. Cai, C.C. Chu, G. Liu, Y.X.J. Wang (2015), "Metal-Organic Framework-Based Nanomedicine Platforms for Drug Delivery and Molecular Imaging", *Small*, **11**, pp.4806-4822.

[8] M. Zheng, S. Liu, X. Guan, Z. Xie (2015), "One-Step Synthesis of Nanoscale Zeolitic Imidazolate Frameworks with High Curcumin Loading for Treatment of Cervical Cancer", *ACS Applied Materials & Interfaces*, **7**, pp.22181-22187.

[9] S. Jiang, Y. Zhang, K.M. Lim, E.K.W. Sim, L. Ye (2009), "NIR-to-visible up-conversion nanoparticles for fluorescent labeling and targeted delivery of siRNA", *Nanotechnology*, **20**, doi: 10.1088/0957-4484/20/15/155101.

[10] C. Wang, L. Cheng, Z. Liu (2011), "Drug delivery with up-conversion nanoparticles for multi-functional targeted cancer cell imaging and therapy", *Biomaterials*, **32**, pp.1110-1120.

[11] S. Chen, Q. Zhang, Y. Hou, J. Zhang, X.J. Liang (2013), "Nanomaterials in medicine and pharmaceuticals: nanoscale materials developed with less toxicity and more efficacy", *Eur. J. Nanomed.*, **5**, pp.61-79.

[12] C. Wang, L. Cheng, Z. Liu (2013), "Up-conversion Nanoparticles for Photodynamic Therapy and Other Cancer Therapeutics", *Theranostics*, **3**, pp.317-330.

[13] Y. Li, J. Tang, L. He, Y. Liu, Y. Liu, C. Chen, Z. Tang (2015), "Core-Shell Up-conversion Nanoparticle@Metal-Organic Framework Nanoprobes for Luminescent/Magnetic Dual-Mode Targeted Imaging", *Adv. Mater.*, **27**, pp.4075-4080.

[14] K. Deng, Z. Hou, X. Li, C. Li, Y. Zhang, X. Deng, Z. Cheng, J. Lin (2015), "Aptamer-Mediated Up-conversion Core/MOF Shell Nanocrystals for Targeted Drug Delivery and Cell Imaging", *Scientific Reports*, **5**, doi: 10.1038/srep07851.

[15] T.K.G. Lam, K.A. Tran, T.B. Nguyen, Q.M. Le, L. Marciniak, W. ojkowski (2015), "Fabrication and up-conversion emission processes in nanoluminophores $NaYF_4$: Er, Yb and $NaYF_4$: Tm, Yb", *Int. J. Nanotechnol.*, **12**, pp.538-547.

[16] A. Patterson (1939), "The Scherrer Formula for X-Ray Particle Size Determination", *Physical Review*, **56(10)**, pp.978-982.

[17] M. Wickenheisser, T. Paul, C. Janiak (2016), "Prospects of monolithic MIL-MOF@ poly(NIPAM)HIPE composites as water sorption materials", *Microporous and Mesoporous Materials*, **220**, pp.258-269.

[18] S. Cao, T.D. Bennett, D.A. Keen, A.L. Goodwind, A.K. Cheetham (2012), "Amorphization of the prototypical zeolitic imidazolate framework ZIF-8 by ball-milling", *Chem. Commun.*, **48**, pp.7805-7807.

[19] J. Li, Y. Wu, Z. Li, B. Zhang, M. Zhu, X. Hu, Y. Zhang, F. Li (2014), "Zeolitic Imidazolate Framework-8 with High Efficiency in Trace Arsenate Adsorption and Removal from Water", *J. Phys. Chem. C*, **118**, pp.27382-27387.

[20] B.H. Stuart (2004), *Infrared Spectroscopy: Fundamentals and Applications*, 244p.

[21] R. Pazik, M. Maczka, M. Malecka, L. Marciniak, A. Ekner-Grzyb, L. Mrowczynska, R.J. Wiglusz (2015), "Functional up-converting $SrTiO_3$:Er^{3+}/Yb^{3+} nanoparticles:structural features, particle size, colour tuning and in vitro RBC cytotoxicity", *Royal Society of Chemistry.*, **22**, pp.10267-10280.